European Journal of Pharmaceutical Sciences 213 (2025) 107235

Contents lists available at ScienceDirect

European Journal of Pharmaceutical Sciences

journal homepage: www.elsevier.com/locate/ejps

Pharmacokinetics, metabolism, and toxicity of anisomelic acid and ovatodiolide: Guiding route of administration in preclinical studies

Navid Delshad [a,b], Preethy Paul [a,b,*], Michael Santos Silva [a,b], Emrah Yatkin [c], Mikko Voipio [c], Senthil Kumar Rajendran [a,b], John E. Eriksson [a,b,*]

[a] Cell Biology, Biosciences, Faculty of Science and Engineering, Åbo Akademi University, Turku FI-20520, Finland
[b] Turku Bioscience Centre, University of Turku and Åbo Akademi University, Turku FI-20520, Finland
[c] Central Animal Laboratory, University of Turku, Turku FI-20520, Finland

ARTICLE INFO

Keywords:
Pharmacokinetics
Anisomelic acid
Ovatodiolide
Metabolism
Bioavailability
Toxicity

ABSTRACT

Despite extensive progress in cancer therapeutic research, translating promising anticancer compounds into clinical treatments often fails due to suboptimal pharmacokinetic and safety profiles. These shortcomings underscore the critical need for comprehensive pharmacokinetic (PK) analyses in the early stages of drug development. Among the compounds that have shown promising anticancer effects in multiple preclinical studies are anisomelic acid (AA) and ovatodiolide (OVT) — two diterpenoids from plant *Anisomeles malabarica*. However, their pharmacokinetic and toxicity profile remain poorly characterized. To explore their potential as chemotherapy agents, we first evaluated their key *in vitro* pharmacokinetic (PK) parameters, followed by an acute oral toxicity assessment and complementary *in vivo* PK analyses. *In vitro* experiments showed that both AA and OVT exhibited near-complete solubility in phosphate buffer, high stability, and strong permeability across MDR1-MDCK cell monolayer, and were not substrates of multidrug resistance protein (MDR1). However, OVT underwent rapid metabolism in liver microsomes in the presence of NADPH, whereas AA showed comparatively greater stability under the same conditions. Subsequent *in vivo* pharmacokinetic (PK) analyses in mice also demonstrated rapid clearance and low systemic bioavailability for both compounds following intravenous (IV) or transdermal (TD) administration. Metabolite identification revealed extensive conjugation to cysteine, and no acute toxicity or mortality was observed at high oral doses. Collectively, these data underscore the distinct metabolic and clearance patterns that limit systemic bioavailability but highlight the favorable safety of AA and OVT. Moreover, while topical administration may offer therapeutic advantages for localized conditions, additional formulation strategies will be crucial to overcome limited bioavailability for systemic use of AA or OVT.

1. Introduction

Bioactive compounds derived from medicinal plants remain an important source of therapeutic agents, either used directly as drugs or as templates for novel drug development, particularly in cancer treatment (Hui et al., 2024). Among these, AA and OVT isolated from Anisomeles malabarica, exhibit a broad range of therapeutic activities (Bhuvaneshwari and Anandhan, 2024; Santhanalakshmi et al., 2024) and have been extensively studied for their anticancer properties (Hou et al., 2009; Preethy et al., 2013; Paul et al., 2014; Lu et al., 2016; Chang et al., 2018; Liu et al., 2019; Huang et al., 2020; Ou et al., 2020; Wu et al., 2020).

While several studies have explored the molecular mechanisms of action of AA and OVT, comprehensive evaluations of their pharmacokinetic suitability as potential drugs, remain limited. To date, only one study has assessed the toxicity of OVT in a rat model (Chen et al., 2021) which provides toxicologic insights, but lacks some critical pharmacokinetic data.

Although AA and OVT belong to the macrocyclic cembrane diterpenoid class and share a common structural backbone, they differ in their functional groups and side-ring structures as illustrated in Fig. 1.

Given their shared macrocyclic cembrane diterpenoid backbone, the presence of electrophilic α,β-unsaturated carbonyl groups, and overlapping reports of anticancer and pro-apoptotic effects— particularly in HPV-transformed cells—we aimed to investigate how subtle structural differences between AA and OVT influence their pharmacokinetic

* Corresponding authors at: Cell Biology, Biosciences, Faculty of Science and Engineering, Åbo Akademi University, Turku FI-20520, Finland.
E-mail addresses: paul.preethy@abo.fi (P. Paul), john.eriksson@abo.fi (J.E. Eriksson).

https://doi.org/10.1016/j.ejps.2025.107235
Received 24 April 2025; Received in revised form 31 July 2025; Accepted 11 August 2025
Available online 12 August 2025

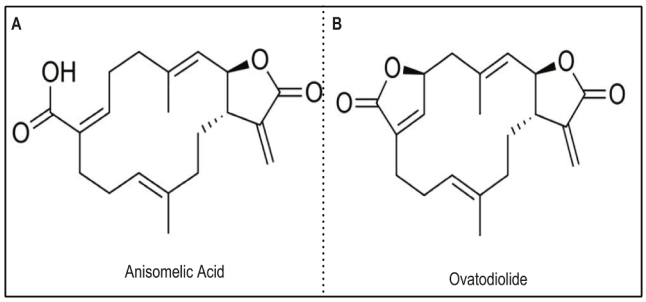

Fig. 1. Two-dimensional structure of AA (PubChem CID: 5358705) and OVT (PubChem CID: 38347030). AA contains a free carboxylic acid group, whereas in OVT, the corresponding carboxylic acid forms a lactone ring through intramolecular cyclization.

profiles and translational potential. To address these questions, we first performed *in vitro* assays, to evaluate solubility, stability, permeability, and metabolic stability of both compounds. Following, we conducted an acute high-dose oral toxicity study in mice before proceeding to *in vivo* PK analysis. Finally, we characterized PK profiles and identified metabolites in mice following intravenous (IV) and transdermal (TD) administration. Our findings will help refine preclinical studies and make informed decisions about potential use cases and optimal routes of administration for these compounds.

2. Materials and methods

2.1. Reagents and test compounds

All reagents, solvents, and cell culture supplies were purchased from Sigma-Aldrich (St. Louis, MO, USA) or Thermo Fisher Scientific (Waltham, MA, USA), unless otherwise noted. The compounds AA (batch No. L22017-B, purity ≥ 98%) and OVT (batch No. L22017-D, purity ≥ 98%) were provided by Anison Therapeutics (Turku, Finland). Both compounds were received as a fine yellowish-white powder and were either kept in their solid form or dissolved in DMSO to create a 100 mM stock solution for further use. In both forms, the compounds were stored at -20°C.

2.2. Chromatographic and mass spectrometric instrumentation

For the fractionation of analytes in all experiments, a Waters ACQUITY UPLC system (Waters™, Milford, MA, USA) was used. For the quantification of OVT levels in *in vivo* pharmacokinetic studies, a Waters Xevo TQ-S triple quadrupole mass spectrometer (Waters™, Milford, MA, USA) was employed. OVT metabolite identification was conducted using a Thermo Scientific Orbitrap Exploris 120 system (Thermo Fisher Scientific, Waltham, MA, USA). All other mass spectrometric analyses were performed using a Thermo Scientific Q Exactive Orbitrap system (Thermo Fisher Scientific, Waltham, MA, USA). Detailed information on chromatographic conditions, including column specifications and mobile phase compositions, is available in the raw data repository (see Data Availability section).

2.3. Kinetic solubility in phosphate buffer

To assess the kinetic solubility of compounds, a 200 μM solution of each compound was prepared from 10 mM stock solution in phosphate buffer (pH 7.4). Subsequently, 500 μL of each solution was transferred into a Whatman™ Mini-UniPrep™ syringeless filter vial (GE Healthcare, Whatman™ Product No. UN203NPUORG). The vials were vortexed for two minutes, followed by agitation for 24 h at room temperature. Following agitation, the vials were centrifuged at 4000 rpm for 20 min to separate the dissolved fraction. The integrated plunger filter was then compressed to filter the sample, and the filtrate was directly injected into the UPLC-UV system for analysis. All kinetic solubility experiments were performed in duplicate, and the assay was validated with controls including Amiodarone hydrochloride (poor solubility), Carbamazepine (moderate solubility), and Chloramphenicol (high solubility).

2.4. Stability in phosphate buffer

To assess the stability of AA and OVT in phosphate buffer, 200 μM solutions of each compound were prepared in DMSO. Aliquots corresponding to various incubation time points were then dispensed into a 96-well plate, with each time point measured in duplicate. Phosphate buffer (pH 7.4) was then added to each well to achieve a final compound concentration of 2 μM, while maintaining the DMSO concentration at 1% in the final incubation mixture.

The samples were incubated at 37 °C with shaking at 600 rpm for 0, 1, 2, 6 and 24 h. At each designated time, 400 μL of cold acetonitrile was added to quench the reaction. The quenched mixtures were centrifuged at 4000 rpm at 4 °C for 20 min. Finally, 60 μl of supernatant was diluted with 180 μL of purified water prior to running LC-MS/MS analysis.

The percentage of remaining test compounds was calculated using Eq. (1):

$$\%\ \boldsymbol{Remaining} = (\boldsymbol{PAR_T} / \boldsymbol{PAR_0}) \times 100 \quad (1)$$

where PAR_T represents the peak area ratio (to the internal standard) at a given time point and PAR_0 is peak area ratio at time zero.

2.5. Bi-directional permeability across MDR1-MDCK II cell monolayer

The objective of this experiment was to evaluate the permeability and efflux properties of AA and OVT using an MDR1-MDCKII cell monolayer model. Nadolol (low permeability marker), Metoprolol (moderate permeability marker), and Digoxin (MDR1 substrate) were included as references to validate the assay.

The MDR1-MDCK II cells (Netherlands Cancer Institute, Amsterdam, Netherland), were cultured on polycarbonate membranes in a 96-well insert system (Corning, Cat REF:3391 and 2533910000) at a density of 3.33×10^5 cells/ml for 6 days in Dulbecco's Modified Eagle Medium (DMEM), supplemented with 10% fetal bovine serum (FBS), 100 IU/mL penicillin and 100 μg/mL streptomycin to form a confluent monolayer.

AA and OVT were diluted with Hanks' Balanced Salt Solution (HBSS) containing HEPES (pH 7.4) from 10 mM DMSO stock solution to a concentration of 2 μM (final DMSO concentration < 1%). These solutions were applied to either apical (A) or basolateral (B) side of the cell monolayer. The plates were incubated for 2.5 h at 37°C with saturated humidity and 5% CO2, without shaking. The permeation of the test compounds from the A to B direction, and vice versa, was determined in duplicate. Following the transport assay, a Lucifer yellow rejection test was performed to assess the integrity of the cell monolayer. LC-MS/MS was used to quantify the analytes.

The apparent permeability coefficient (P_{app}, cm/s) was calculated using Eq. (2):

$$P_{app} = (dC_r/d_t) \times V_r / (A \times C_0) \quad (2)$$

Where dCr/dt is the rate of compound appearance in the receiver chamber over time (μM/s), V_r is the solution volume in the receiver chamber, A is the surface area available for transport, C_0 is the initial concentration in the donor chamber (μM).

The efflux ratio was calculated as in Eq. (3):

$$\text{Efflux Ratio} = P_{app}\ (BA) / P_{app}\ (AB) \quad (3)$$

In which the BA is basolateral to apical, and AB refers to apical to basolateral direction and finally percentage recovery was calculated using the following equation:

$$\% \text{ Recovery} = 100 \times [(V_r \times C_r) + (V_d \times C_d)] / (V_d \times C_0) \quad (4)$$

Where V_d is the volume in the donor chambers, C_d and C_r are the final concentrations in donor and receiver chambers, respectively.

2.6. Metabolic stability in liver microsomes

Microsomal stability assays were performed as an initial screen to evaluate the metabolic liability of AA and OVT *in vitro*. Experiments were conducted using a mixed-gender pool of 150 donors (HLM; Corning, Cat No. 452117, Lot No. 38298) and mouse liver microsomes (MLM; Xenotech Cat No. M1000, Lot No. 2110330). The HLM was a mixture of Cytochrome P450 (CYP2C19, CYP1A2, CYP2C9, CYP2D6, and CYP3A4) and UDP-glucuronosyltransferase (UGT) enzymes, while the MLM was composed of Cytochrome P450 and Cytochrome b_5 enzymes from male CD-1 mouse strain. The tests were conducted in the presence or absence of NADPH (Bontac, Cat No. BT04) as co-factor. To benchmark the metabolic clearance of the test compounds, three reference drugs with well-characterized CYP-mediated metabolism were included as internal controls, testosterone (CYP3A4 substrate), diclofenac (CYP2C9 substrate), and propafenone (CYP2D6 substrate). These compounds represent a spectrum of hepatic metabolic clearance rates (low to high) and were used to validate microsomal activity and provide contextual interpretation of the pharmacokinetic parameters of AA and OVT.

AA and OVT were incubated at a final concentration of 1 μM with 0.5 mg/mL of either human or mouse liver microsomes. The mixtures containing NADPH were incubated at 37°C while shaking for 5, 15, 30, 45, or 60 min, whereas mixtures without NADPH were incubated for 60 min only. After the incubation period, cold AcN was added to terminate the reaction, followed by centrifugation at 4000 rpm for 20 min. The supernatant was then diluted with HPLC-grade water, and further analysis was conducted using LC-MS/MS.

The first-order kinetic equation was used to calculate $T_{1/2}$ (half-life):

$$C_t = C_0 \times e^{-k_e \times t} \quad (5)$$

Where C_t is the concentration of compound at time t, C_0 is the initial concentration of the compound, K_e is the first order elimination rate constant.

In addition, the intrinsic microsomal clearance (CL_{mic}, μl/min/mg) was calculated as in Eq. (6):

$$CL_{mic} = (k_e \times 1000) / \text{MPM} \quad (6)$$

MPM refers to microsomal protein mass, in milligrams per milliliter of reaction volume. Liver intrinsic clearance (CL_{liver}) was estimated using the derived values of microsomal clearance:

$$CL_{liver} = CL_{mic} \times (\text{MPM} / \text{LW}) \times (\text{LW/BW}) \quad (7)$$

LW stands for liver weight in grams and BW stands for body weight in kilograms. The liver weight to body weight ratio and the microsomal protein per liver weight were chosen according to the manufacturer datasheet.

2.7. In vivo pharmacokinetic profiling and metabolite identification

In this study, AA or OVT, was administered to male FVB/N mice (Charles River Laboratories, Wilmington, MA, USA) either IV or TD. A total of 36 animals were used in this study, with 9 animals assigned to each treatment condition per route (AA IV, AA TD, OVT IV, OVT TD). At 5 weeks of age, animals were weighed and randomly divided into three groups (n = 3 per group) within each treatment arm. The mean body weights at baseline were: AA IV: 22.4 ± 1.1 g, AA TD: 22.8 ± 1.1 g, OVT IV: 22.2 ± 2.0 g, and OVT TD: 22.8 ± 1.1 g (one-way ANOVA, $p = 0.77$). For IV administration, the compounds were dissolved in a mixture of N-Methyl-2-pyrrolidone (NMP), polyethylene glycol 400 (PEG-400) and Macrogol (15)-hydroxy stearate (Kolliphor® HS 15) and diluted in sterile sodium chloride (9 mg/mL) solution for injection, filtered and administered with a final dose of 1 mg/kg. For TD administration, an ointment containing 20% (w/w) of the active compound in white petroleum (Medifon Oy, Espoo, Finland) was applied as 4 mg of cream per gram of animal body weight. For the application, the fur on the back of the animals' necks was shaved, and the cream was applied to an area of approximately 2 cm^2.

Blood sampling via saphenous vein (SV) was performed at staggered time points to minimize total blood volume collected per animal: Group 1 was sampled at 5, 30, and 240 min post-dose; Group 2 at 15, 120, and 1440 min; and Group 3 at 60, 480, and 600 min. At each time point, 50 μL of blood was collected and plasma was immediately separated by centrifugation at 2700 × g for 10 min. The test samples were prepared by mixing 10 μL of plasma with 50 μL precipitation solution (AcN with 1% FA). The samples were mixed for 3 min, then centrifuged for 20 min at 2000 g. The supernatant was transferred to an analytical plate, diluted 1:1 with ultrapure water, and submitted for analysis. Standard samples were prepared by spiking blank male FVB mouse plasma (5 μL standard and 45 μL blank plasma) to achieve analyte concentrations ranging from 0.1 ng/mL to 10,000 ng/mL. For metabolite identification, an additional 10 μL aliquot of plasma samples were used.

Bioavailability (BA), expressed as a percentage, was derived by using Eq. (8):

$$BA = (AUC_{0\text{-}\infty\ TD} / AUC_{0\text{-}\infty\ IV}) \times (\text{Dose IV/Dose TD}) \times 100 \quad (8)$$

Where AUC is area under the curve and clearance (CL) was calculated using Eq. (9):

$$CL = \text{Dose}/ AUC_{0\text{-}\infty\ IV} \quad (9)$$

The mean residence time (MRT), indicating the average time a drug molecule remains in the body, was determined by:

$$MRT = AUMC/AUC \quad (10)$$

where AUMC is the area under the moment curve and AUC is area under the curve.

The volume of distribution at steady state (V_{ss}), which estimates the extent of drug distribution in the body relative to the plasma, was obtained by:

$$V_{ss} = CL \times MRT \quad (11)$$

2.8. Acute toxicity

An acute toxicity study was conducted in accordance with OECD Guideline 420 (OECD, 2002) for acute oral toxicity using a fixed-dose procedure.

Female C57BL/6 Clr mice (Charles River Laboratories, Wilmington, MA, USA) were housed in individually ventilated cages (Tecniplast, Italy). One mouse was first used in a sighting study at 300 mg/kg according to OECD Test Guideline 420. Since no mortality or severe toxicity was observed within 24 h, an additional five mice were administered a dose of 2000 mg/kg for the main study. The room temperature was between 18 and 24°C, with relative humidity maintained between 30 and 70%, and the lighting followed a 12-hour day/night cycle (7 am to 7 pm). Water and food were available to the animals ad libitum.

For dosage preparation, AA and OVT were initially dissolved in pure ethanol and then diluted with corn oil to form a suspension, resulting in a final ethanol concentration of 20%. The suspensions were prepared to ensure that the administered volume did not exceed 250 μL per dose. The test items were administered as a single intragastric dose.

Prior to dosing, the animals were fast for 4 h, during which only food was withheld while water remained accessible. Food was withheld for an additional hour post-dosing. After dosing, the animals were observed twice daily for 14 days to monitor for any clinical signs of toxicity.

Clinical observations focused on behavioral changes, signs of pain or distress, and any physiological abnormalities. Body weights were recorded prior to dosing and on days 2, 7, and 14 post-dosing. Ponderal gain was calculated as follows:

$$\text{Ponderal gain \%} = [(W_2 - W_1) / W_1] \times 100 \quad (12)$$

where W_1 represents the initial body weight and W_2 represents the body weight on day 14.

3. Data analysis and visualization

Data processing and plotting were performed using Python (version 3.12.6), with the pandas and matplotlib.pyplot libraries or GraphPad Prism (version 7; GraphPad Software, San Diego, CA, USA). Chromatographic and metabolite data were processed and visualized using MassLynx 4.2 (Waters™, Milford, MA, USA), Thermo Xcalibur 4.1.31.9, and Compound Discoverer 2.1 (Thermo Fisher Scientific, Waltham, MA, USA) software.

4. Results

4.1. AA and OVT are moderately soluble in phosphate buffer with DMSO as co-solvent

Table 1 summarizes the kinetic solubility data for AA, OVT, and the validation controls. Both AA and OVT showed moderate solubility under these conditions, comparable to carbamazepine, the moderate-solubility control. As expected, amiodarone level was below the limit of quantification (LOQ), indicating poor solubility, whereas chloramphenicol was fully soluble (≥ 200 μM).

4.2. AA shows minor degradation (≥ 90% retained) while OVT remains over 99.5% stable in phosphate buffer over 24 h

AA levels showed a slight decrease but remained above 90% throughout the duration of the study, while OVT remained completely stable for the first 6 h, with only a 0.5% decrease observed after 24 h. The percentage remaining for both AA and OVT is shown in Fig. 2.

4.3. AA and OVT have intermediate permeability and are not MDR1 substrates

As shown in Table 2, the mean apparent permeability coefficient (P_{app}) in the apical-to-basolateral direction (A to B) was 13.3×10^{-6} cm/s for AA and 12.8×10^{-6} cm/s for OVT. In the basolateral-to-apical direction (B to A), AA and OVT showed mean P_{app} values of 6.67×10^{-6} cm/s and 8.01×10^{-6} cm/s respectively.

Evaluation of the mean solution recovery percentages indicated that 40.6 % of AA and 37.8 % of OVT were recovered from the apical-to-basolateral direction, while recoveries in the basolateral-to-apical direction were 77.9% for AA and 68.5% for OVT.

Table 1
Kinetic solubility of AA, OVT, and controls (phosphate buffer, pH 7.4, 2% DMSO). Amiodarone hydrochloride (poor solubility), carbamazepine (moderate solubility), and chloramphenicol (high solubility) were used as different representative of solubility categories . Data is presented as mean ± SD (n=2).

Compound	Target Concentration (μM)	Kinetic Solubility (μM)
Anisomelic Acid	200	174.42 ± 0.64
Ovatodiolide	200	174.9 ± 0.0
Amiodarone HCl	200	< LLOQ [1]
Carbamazepine	200	171.3 ± 0.32
Chloramphenicol	200	≥ 200

[1] Below the lower limit of quantification.

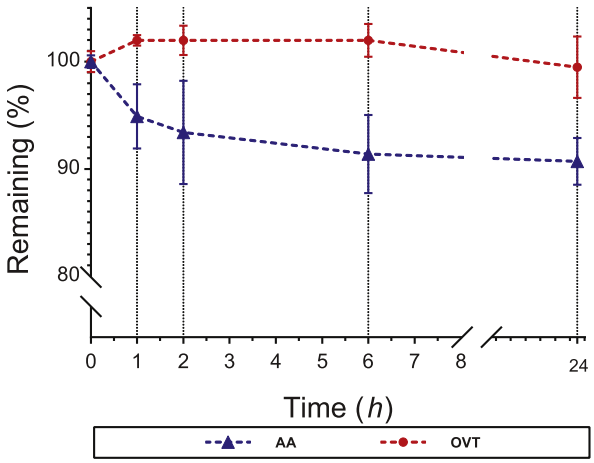

Fig. 2. Stability of AA and OVT in phosphate buffer. AA showed minor degradation, with concentration remaining over 90% while OVT remained over 99.5% throughout the 24-hour period.

Table 2
Apparent permeability coefficient (P_{app}) and efflux ratio of AA and OVT through MDR1-MDCK II Cell Monolayer. Nadolol (low permeability marker), metoprolol (high permeability marker) and digoxin (MDR1 substrate), were used as validation controls. Data is presented as mean ± SD (n=2).

	P_{app} (10^{-6} cm/s)		Solution Recovery %		Efflux Ratio
	A to B[1]	B to A	A to B	B to A	
Anisomelic Acid	13.3 ± 0.2	6.67 ± 0.0	40.6 % ± 0.88	77.9 % ± 0.68	0.5 ± 0.0
Ovatodiolide	12.8 ± 0.08	8.01 ± 0.17	37.8 % ± 0.0	68.5 % ± 1.34	0.62 ± 0.0
Nadolol	0.135 ± 0.02	< LLOQ[2]	91.8 % ± 0.88	< LLOQ	< LLOQ
Metoprolol	22.6 ± 1.33	< LLOQ	85.7 % ± 3.98	< LLOQ	< LLOQ
Digoxin	0.438 ± 0.03	7.91 ± 0.63	88.7 % ± 1.4	96.0 % ± 5.86	18.04 ± 0.32

[1] A = Apical, B=Basolateral
[2] Below the lower limit of quantification

4.4. OVT undergoes rapid NADPH-dependent metabolism, while AA displays species-dependent stability in liver microsomes

The metabolic stability of AA and OVT was evaluated in human liver microsomes (HLM) and mouse liver microsomes (MLM). The percentage of compound remaining over time is illustrated in Fig. 3. OVT showed rapid NADPH-dependent degradation in both HLM and MLM, with near-complete elimination occurring within minutes. In contrast, AA exhibited slower metabolic turnover, particularly in HLM, where over 75% of the compound remained after 60 min of incubation.

In vitro pharmacokinetic parameters derived from first-order exponential decay fitting are summarized in Table 3. The data confirms NADPH-dependent metabolism for both compounds *in vitro*, as only minimal degradation was observed in control incubations lacking NADPH.

4.5. Rapid IV clearance and prolonged TD exposure of AA and OVT in vivo

Fig. 4 illustrates the plasma concentration profiles of AA and OVT following IV and TD administration.

As shown in Table 4, AA was rapidly cleared from systemic circulation following IV administration, with a half-life ($T_{½}$) of 0.0634 h (3.8 min). In contrast, TD application of AA resulted in a delayed T_{max} of 5 h,

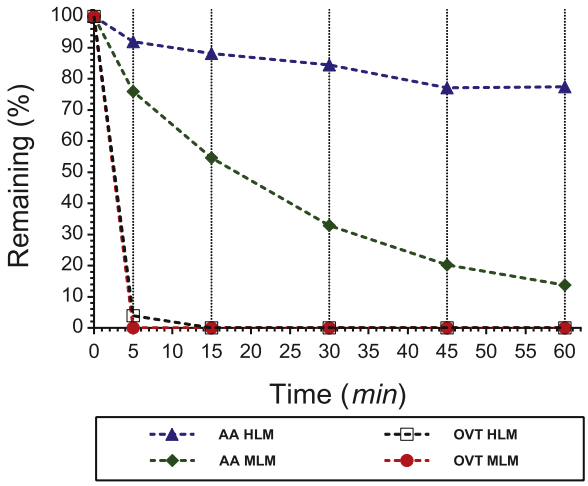

Fig. 3. Metabolic stability of AA and OVT in human liver microsomes (HLM) and mouse liver microsomes (MLM). OVT underwent rapid metabolic degradation, with near-complete elimination within minutes in both HLM and MLM. In contrast, AA exhibited a slower rate of degradation, particularly in HLM.

a higher C_{max} and an increased mean residence time (MRT). The bioavailability of AA from the TD formulation was 4.37%.

OVT also exhibited a rapid systemic clearance following IV administration with half-life of 0.255 h (15.3 min). After TD administration, OVT reached its Cmax after 1 h, lower Cmax compared to AA, an MRT of 8.26 h, and a bioavailability of 0.19%.

4.6. Primary metabolic pathway of AA and OVT in both IV and TD in vivo: reduction followed by cysteine conjugation

As shown in Fig. 5, IV administration of AA resulted in rapid metabolism within the first 5 min, with the majority of detectable metabolites arising from both Phase I (e.g., double-bond reduction, oxidation) and Phase II reactions (notably cysteine conjugation). Double-bond reduction followed by cysteine cleavage and methylation emerged as the dominant metabolic route for AA. In contrast, OVT primarily underwent double-bond reduction followed by GSH and cysteine conjugation, with a relatively narrower metabolite profile in IV samples.

In TD administration, both AA and OVT showed a broader spectrum of metabolic transformations. Notably, extensive Phase I oxidation, dehydrogenation, and multi-step conjugation (including glucuronidation and thiol methylation) were observed. AA exhibited greater metabolic diversity, including inferred and confirmed downstream metabolites with multiple oxidation and conjugation layers. Among OVT metabolites, M8 ($C_{26}H_{35}NO_{11}$) was identified as a glucuronidated product likely formed via an N-conjugated intermediate of oxidized OVT. Detailed identification and characterization of all detected metabolites, including their proposed biotransformations, chemical formulas, retention times, and m/z values, are summarized in Supp. Table 1 and Supp. Table 2 for AA and OVT, respectively.

The proposed metabolic schemes (Fig. 6) summarize the major routes for each compound, including inferred intermediates, thiol-processing cascades (GSH → Cys-Gly → Cys → Cys-D), and observed Phase II derivatization patterns. Time-dependent accumulation and relative abundance of metabolites by absolute peak area, are shown in Supp. Fig. 1.

4.7. High oral doses of AA and OVT show no observable toxicity in mice

No mortality or clinical signs of toxicity were observed in any animal during either the sighting (300 mg/kg) or main phase (2000 mg/kg) of the acute oral toxicity study following the oral administration of AA or OVT. All animals survived the 14-day observation period without adverse behavioral or physiological symptoms. Body weight monitoring indicated a general trend of positive weight gain across both treatment groups (see Supp. Fig. 2). Clinical observations included assessment of general appearance (skin, fur, and mucous membranes), posture, locomotor and behavioral activity, respiratory pattern, and autonomic signs such as salivation or piloerection—none of which were observed in any treated animal. At necropsy, macroscopic examination of major organs including the liver, kidneys, lungs, heart, spleen, and gastrointestinal tract revealed no visible abnormalities or morphological changes. These findings support an estimated $LD_{50} > 2000$ mg/kg and indicate that the test compounds are not subject to classification under any acute oral toxicity category of the Globally Harmonized System (GHS).

5. Discussion

Our study explains the pharmacokinetic and safety profiles of AA and OVT, two naturally derived compounds from *Anisomeles malabarica* plant that have been traditionally used to treat various ailments. Their recently reported antiproliferative effects, especially against HPV-positive cancer cell lines, suggest therapeutic potential, prompting our investigation into their kinetic and safety properties as a foundation for future dosage form development and selecting optimal administration routes. While both compounds were studied in parallel, AA served as the primary compound of interest, with OVT included as a structurally related comparator to contextualize PK and metabolic findings.

Low aqueous solubility is a well-documented limitation among macrocyclic cembrane diterpenoids, causing a significant challenge in their pharmaceutical development due to poor bioavailability and complex pharmacokinetics (de Souza et al., 2024; Zhang et al., 2025). These limitations are often attributed to the large hydrophobic rings of the compounds, despite the sporadic presence of polar functional groups. AA and OVT, both macrocyclic cembrane diterpenoids, exhibit

Table 3
In vitro hepatic metabolic stability and clearance of AA and OVT in human and mouse liver microsomes, with reference to CYP-control substrates.

		R^2	$T_{1/2}$ (*min*)	CL_{mic} (*μL/min/mg*)	CL_{liver} (*mL/min/kg*)	Remaining (*%, T = 60 mins*)	
						With NADPH	No NADPH
Anisomelic Acid	HLM	0.9025	>145[1]	<9.6	<8.6	77.4	92.3
	MLM	0.9945	21.2	65.4	259.1	13.8	92.9
Ovatodiolide	HLM	1.0000	1.07	1295.7	1166.2	0.0	90.7
	MLM	0.0000	< LLOQ [2]	-	-	0.0	91.9
Testosterone	HLM	0.9974	16.2	85.4	76.8	7.5	90.0
	MLM	0.9268	7.0	197.2	780.9	0.3	89.4
Diclofenac	HLM	0.9986	5.9	236.4	212.8	0.1	95.5
	MLM	0.9973	42.6	32.5	128.7	36.9	92.7
Propafenone	HLM	0.9519	5.6	246.0	221.4	0.1	95.2
	MLM	0.9966	1.8	750.1	2970.4	0.1	99.4

[1] Estimated from extrapolation
[2] Below the lower limit of quantification

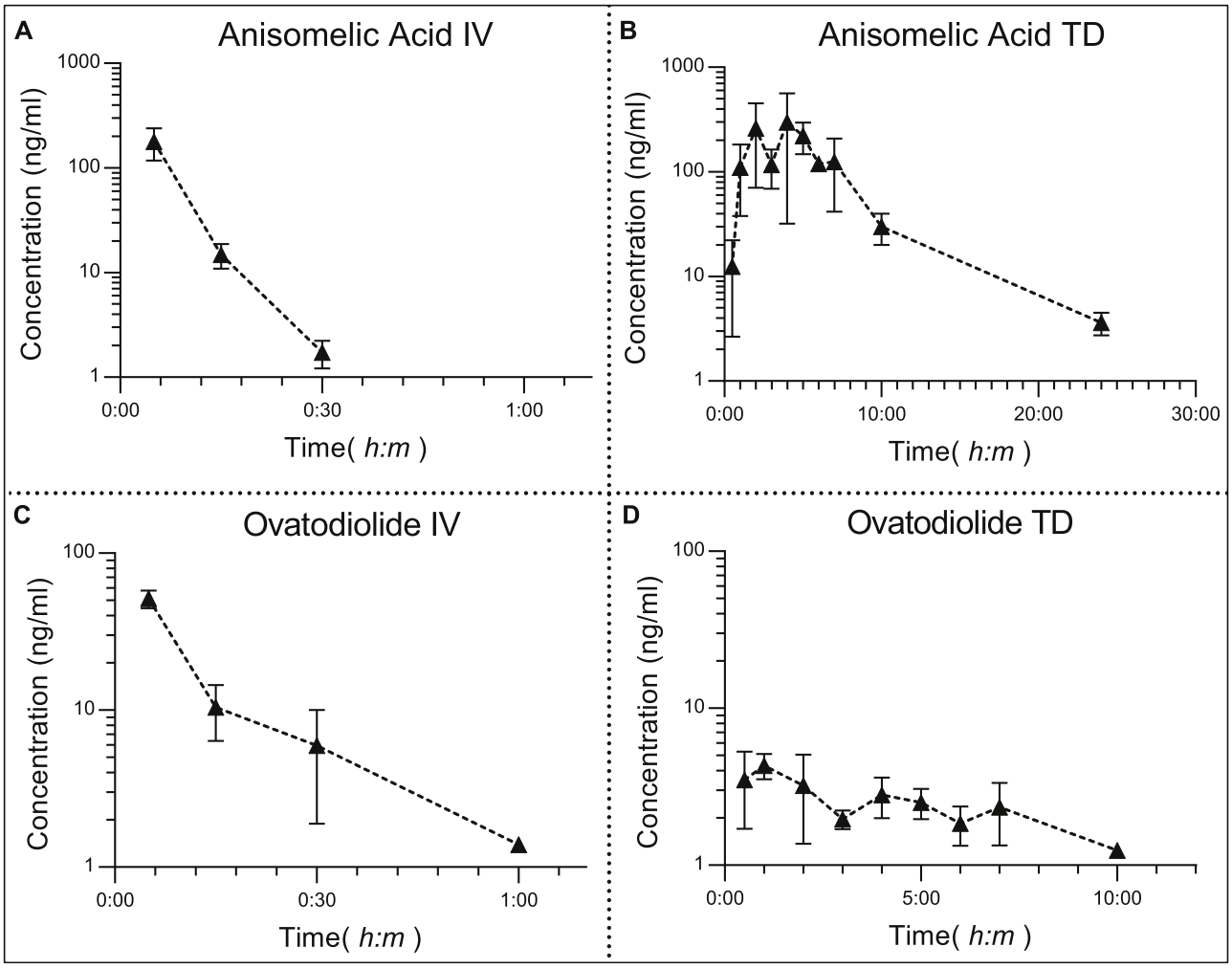

Fig. 4. . Plasma concentrations of AA and OVT following IV (A, C) and TD (B, D) administration. Both compounds exhibited rapid elimination after IV dosing, while TD delivery resulted in a more gradual decline in plasma concentrations.

Table 4
. *In vivo* PK parameters for AA and OVT (Cmax as mean ± SD, n=3).

Compound	Route	C_0 (*ng/mL*)	C_{max} (*ng/mL*)	T_{max} (*h*)	$T_{1/2}$ (*h*)	$AUC_{0-\infty}$ (*h.ng/mL*)	MRT [1] (*h*)	CL[2] (*mL/min/kg*)	BA[3] (%)
AA	IV	616 [4]	178.67 ± 60.93	0.083	0.0634	42	0.0727	397	–
	TD	–	221.33 ± 73.79	5	3.37	1540	5.9	–	4.37
OVT	IV	113	51.27 ± 6.62	0.083	0.255	14.8	0.227	1120	–
	TD	–	4.32 ± 0.79	1	5.39	33.3	8.26	–	0.19

[1]Mean Residence Time
[2] Clearance
[3] Bioavailability
[4] Estimated by back-extrapolation from early time points.

similar physicochemical properties.

In our solubility assay, both compounds demonstrated moderate solubility in phosphate buffer (pH 7.4) containing 2% DMSO, comparable to the moderate-solubility control, carbamazepine. This observation, consistent with other compounds in the same class and our previous data on the solubility of these compounds (Eriksson et al., 2018; Rajendran et al., 2020), reflects their predominantly non-polar structures, containing a single polar moiety. It is important to note that the observed solubility was achieved in the presence of 2% DMSO indicating that the reported values do not represent the intrinsic solubility of AA and OVT.

From a formulation perspective, these findings highlight the importance of including co-solvents as a crucial component in the formulation design for both compounds. This strategy was implemented in our *in vivo* IV formulation, where multiple co-solvents were used to prevent potential precipitation following injection into a biological system, while maintaining DMSO levels below the toxic dose for animals.

In stability studies, both compounds remained largely intact over the test period; however, AA showed minor degradation, likely due to

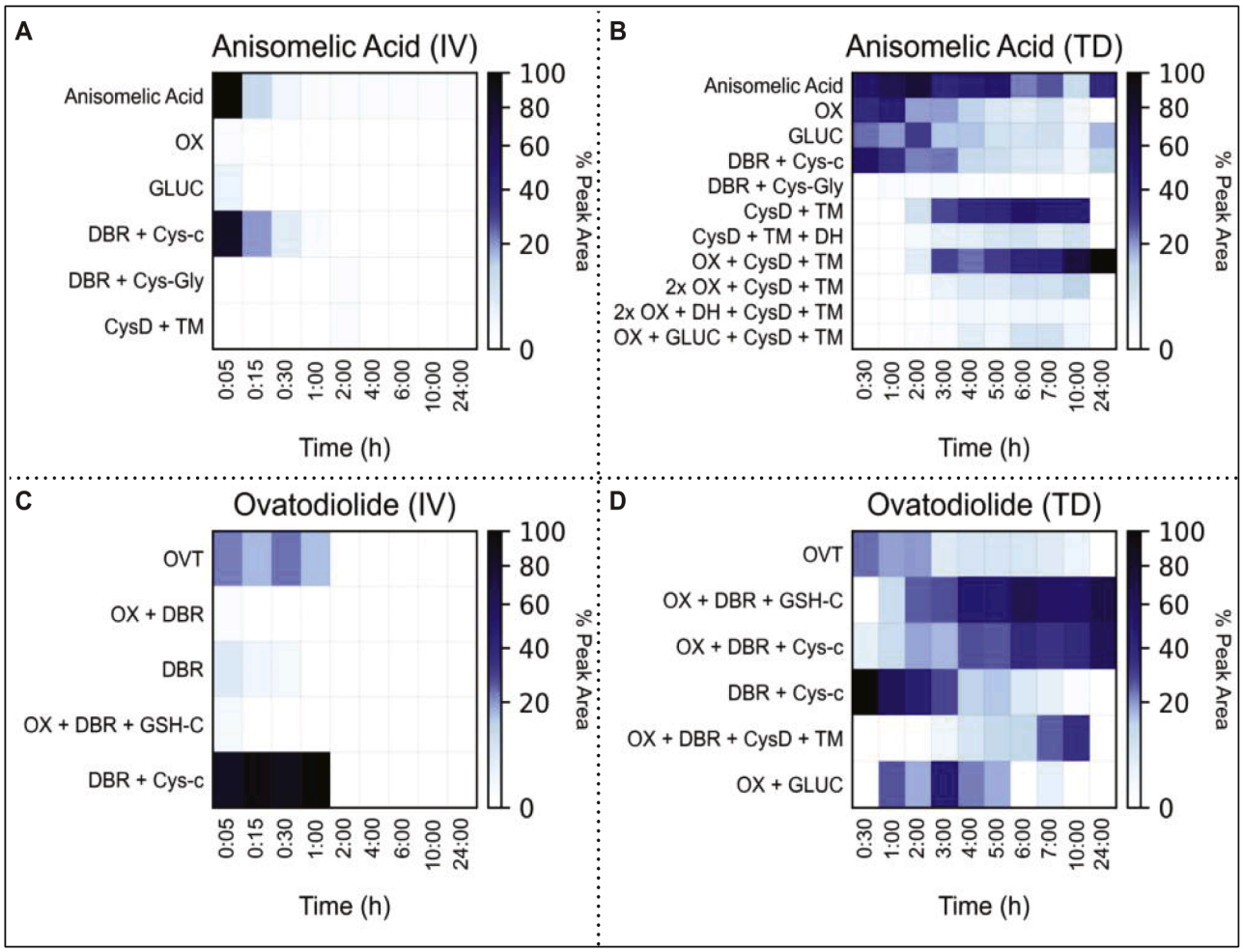

Fig. 5. Metabolic profiling of AA and OVT after IV and TD administration. Heatmaps show the relative abundance (% peak area) of detected metabolites over time. IV administration of AA (A) led to rapid formation of Phase I (e.g., double-bond reduction) and Phase II (e.g., cysteine conjugation) metabolites. TD delivery (B) produced a broader range of metabolites, including glucuronides and dehydrogenated forms. OVT metabolism via IV (C) was dominated by GSH and cysteine conjugates, while TD (D) revealed greater metabolic diversity with additional conjugation and oxidative changes. (OX = Oxidation; DBR = Double Bond Reduction; GSH-C = Glutathione Conjugation; Cys-c = Cysteine Conjugation; Cys-Gly = Cysteine-Glycine Conjugation; CysD = Cysteine Degradation; TM = Thiol Methylation; GLUC = Glucuronidation; DH = Dehydrogenation).

hydrolysis of its lactone ring facilitated, by its free carboxylic acid group (Fersht and Kirby, 1967). Occasional slight increases in OVT concentration were observed but these are most likely due to analytical variability, as confirmed by consistent reference controls and acceptable coefficient of variation (CV%) values.

Both compounds showed moderate permeability, with apparent permeability values between those of low- and high-permeability controls, suggesting some ability to cross biological membranes. The low efflux ratios for AA (0.50) and OVT (0.62) indicate minimal P-glycoprotein (MDR1)-mediated efflux. This is promising, considering the role of MDR1 overexpression in multidrug resistance (Al-Thubiani, 2023; Emran et al., 2022) and could be indicative of a favorable absorption in oral administration from intestinal tract.

In liver microsomes, AA demonstrated relatively high metabolic stability, particularly in human liver microsomes, while OVT was rapidly metabolized in both human and mouse systems. The faster clearance of AA in mouse liver microsomes highlights species-specific differences that may affect the translation of pharmacokinetic findings from mice to humans. Moreover, the rapid metabolism of both compounds may suggest intracellular retention or metabolism, potentially contributing to the recovery rates observed in the permeability assays.

It should also be noted that the *in vitro* metabolic stability assays were conducted early in the study to provide a preliminary assessment of metabolic liability prior to *in vivo* pharmacokinetic evaluation. As such, incubation conditions were not further optimized for compounds with high clearance, such as OVT, and technical replicates were not included at this exploratory stage. However, the inclusion of reference compounds with well-characterized CYP-mediated metabolism supported the reliability of the assay. Given that detailed *in vivo* pharmacokinetic analyses were subsequently performed, we believe that repeating the *in vitro* assays under optimized conditions with replicates would not substantially alter the interpretation or provide additional mechanistic insights beyond those already obtained.

In vivo pharmacokinetic profiling revealed rapid clearance and low systemic bioavailability for both compounds following IV and TD administration, consistent *w*ith the known challenges of macrocyclic cembrane diterpenoids. Although AA showed a higher bioavailability (4.3%) than OVT (0.2%), these values remain suboptimal for systemic therapy. This underscores the need for advanced delivery strategies, such as using nanoparticles, depot injections, or prodrug modifications. Previous formulation efforts using prodrugs and structural modifications have attempted to address these limitations with varying degrees of success (Senthilkumar et al., 2019, 2015; Xiang et al., 2020). On the other hand, the limited systemic absorption observed may offer an advantage for topical use, where prolonged local exposure with minimal systemic distribution is often desired.

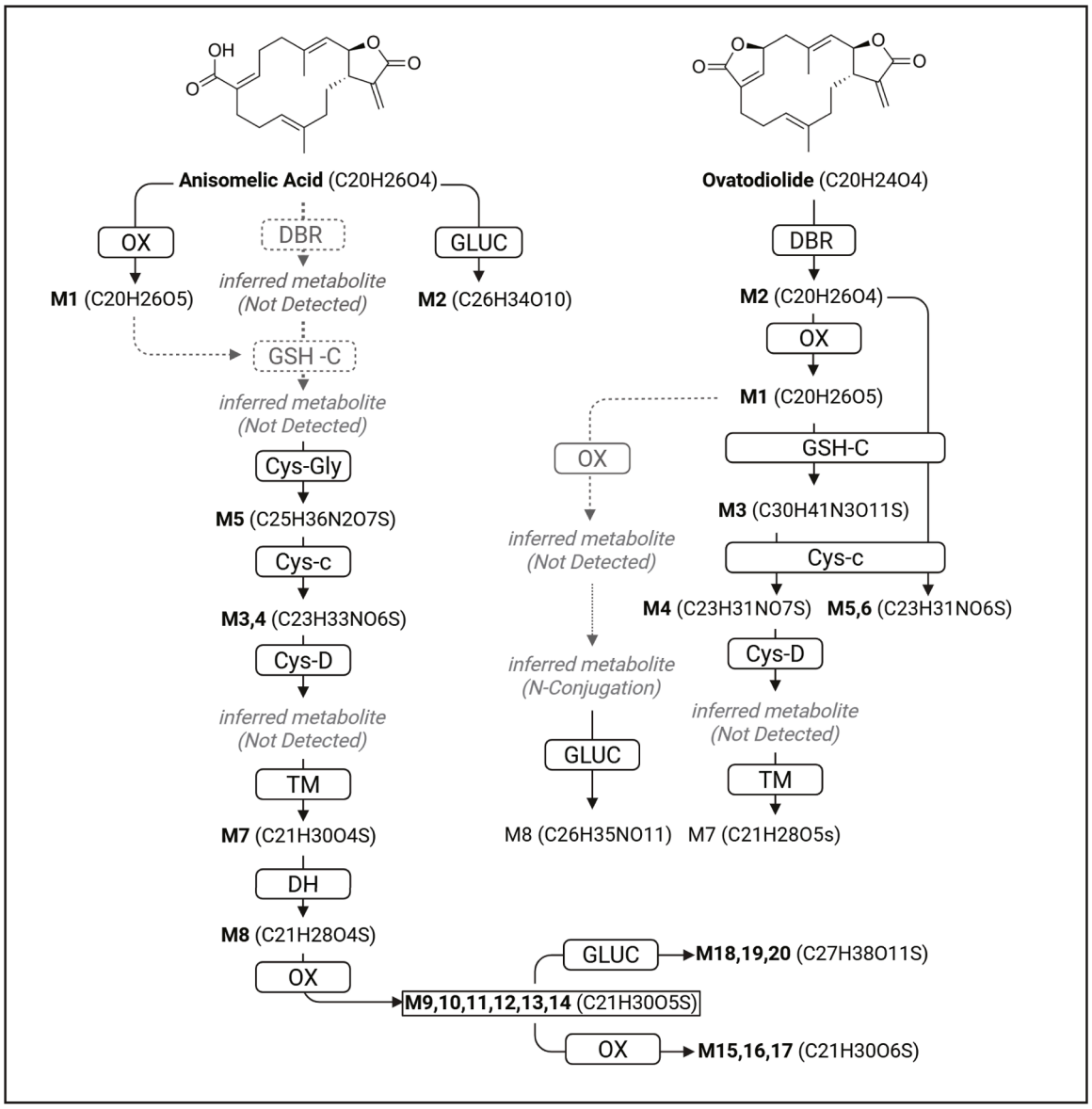

Fig. 6. . Proposed metabolic pathways of AA and OVT *in vivo*. Metabolic routes involve oxidation, double-bond reduction, glutathione and cysteine conjugation, glucuronidation, and downstream modifications including thiol methylation and dehydrogenation. AA exhibited broader metabolic diversity than OVT. M1–M7 (AA) and M1–M6 (OVT) were detected after IV and TD dosing; other metabolites appeared only following TD administration. Dashed and gray arrows indicate inferred intermediates and interactions. (OX = Oxidation; DBR = Double Bond Reduction; GSH-C = Glutathione Conjugation; Cys-c = Cysteine Conjugation; Cys-Gly = Cysteine-Glycine Conjugation; CysD = Cysteine Degradation; TM = Thiol Methylation; GLUC = Glucuronidation; DH = Dehydrogenation).

In addition to rapid metabolic clearance, another factor that may contribute to the low systemic exposure of both AA and OVT is the formation and biliary elimination of Phase II metabolites—particularly acyl glucuronides. Our *in vivo* LC-MS profiling identified glucuronidated metabolites for both compounds (e.g., M2 for AA and M8 for OVT), supporting the activity of UGT-mediated metabolism. Acyl glucuronides are known to be rapidly excreted into bile, thereby potentially bypassing systemic circulation. Since our pharmacokinetic analysis was based solely on plasma samples, this clearance pathway may not have been fully captured, possibly leading to an underestimation of total elimination. This represents a limitation of our study, as bile and fecal samples were not collected to assess non-renal excretory routes. Interestingly, *in vitro* data showed greater metabolic stability for AA in HLM, even though only the human microsomal preparation contained UGT enzymes.

Metabolically, both AA and OVT primarily undergo GSH conjugation *in vivo*, a common metabolic pathway for compounds containing electrophilic centers (Potęga, 2022). This transformation follows the classical mercapturic acid pathway, in which GSH conjugates are sequentially processed through enzymatic cleavage to cysteinyl-glycine, cysteine, and ultimately N-acetylcysteine derivatives. Several metabolites identified in our study—particularly cysteine and cysteine-glycine conjugates—support this biotransformation route.

Notably, a broader and more complex metabolite spectrum was observed following TD administration, including advanced downstream modifications such as glucuronidation, thiol methylation, and additional oxidative transformations. This pattern suggests that cutaneous metabolism—potentially involving skin-localized enzymes such as GSTs, UGTs, and CYPs—may initiate or facilitate metabolic processing (Lau et al., 2024; Quantin et al., 2022). This may pose an additional challenge if the goal is to achieve systemic presence of the compounds after TD application.

Finally, high-dose acute oral toxicity tests revealed no observable toxic effects for either compound. Based on permeability and

pharmacokinetic data, this lack of toxicity is likely not solely attributable to limited absorption, but may also reflect rapid metabolism, efficient elimination and overall low systemic bioavailability.

6. Conclusions

The rapid metabolism, high elimination rate and low systemic bioavailability of AA and OVT suggest that these compounds are not well suited for systemic administration. However, their favorable toxicity profiles, combined with their molecular effects, support their potential for topical use, particularly in the treatment of hyperproliferative and inflammatory epithelial disorders, including HPV-related precancerous lesions. In such context, localized drug delivery may allow therapeutic efficacy while minimizing systemic exposure.

Ethical consideration

All *in vivo* experiments conducted in this study adhered to the guidelines outlined in DIRECTIVE 2010/63/EU of the European Parliament and Finnish national legislation, ensuring high ethical standards, and adhering to the 3Rs principles for animals utilized for scientific research purposes. The acute toxicity experiment was carried out at the Central Animal Laboratory (CAL) of the University of Turku (Turku, Finland), in strict accordance with institutional regulations and standardized operating procedures. The study protocols and procedures were reviewed and approved by the Project Authorization Board of Finland (Care and Use Committee) with license number ESAVI/10594/2022. The *in vivo* pharmacokinetic analysis was done at Admescope Oy, Oulu, Finland (license number ESAVI/35183/2022).

Declaration of generative AI and AI-based technologies in the writing process

In compliance with responsible academic authorship and transparency, we confirm that generative AI tools (e.g., OpenAI's ChatGPT) were employed solely for language editing in this manuscript, focusing on grammar, clarity, and style. All scientific content, data analysis, and conclusions were independently generated by the authors, without alteration by AI tools. No images or figures were created or modified using generative AI.

Glossary

AA, Anisomelic Acid; AcN, Acetonitrile; AUC, Area Under the Curve; AUMC, Area Under the Moment Curve; BW, Body Weight; CL, Clearance; CL_{mic}, Microsomal Clearance; CL_{liver}, Liver Intrinsic Clearance; C_{max}, Maximum Concentration; C_0, Initial Concentration; CV%, Coefficient of Variation (Percent); Cys-c, Cysteine Conjugation; Cys-Gly, Cysteine–Glycine Conjugation; CysD, Cysteine Degradation to Thiol; DBR, Double-Bond Reduction; DH, Dehydrogenation; DMEM, Dulbecco's Modified Eagle Medium; FA, Formic Acid; FBS, Fetal Bovine Serum; GLUC, Glucuronidation; GSH, Glutathione; GSH-C, Glutathione Conjugation; HBSS, Hank's Balanced Salt Solution; HLM, Human Liver Microsomes; HPV, Human Papillomavirus; IV, Intravenous; LW, Liver Weight; MDR1, MultiDrug Resistance Protein 1; MDCK II, MadinDarby Canine Kidney II; MLM, Mouse Liver Microsomes; MPM, Microsomal Protein Mass; MRT, Mean Residence Time; NADPH, Nicotinamide Adenine Dinucleotide Phosphate; NMP, N-Methyl2pyrrolidone; OVT, Ovatodiolide; OX, Oxidation; P_{app}, Apparent Permeability Coefficient; PB, Phosphate Buffer; PEG400, Polyethylene Glycol 400; TD, Transdermal; TM, Thiol Methylation; T_{max}, Time to Reach Maximum Concentration; V_{ss}, Volume of Distribution at Steady State.

CRediT authorship contribution statement

Navid Delshad: Writing – review & editing, Writing – original draft, Visualization, Validation, Methodology, Investigation, Conceptualization. **Preethy Paul:** Writing – review & editing, Writing – original draft, Supervision, Project administration, Methodology, Funding acquisition, Data curation, Conceptualization. **Michael Santos Silva:** Writing – review & editing, Methodology, Conceptualization. **Emrah Yatkin:** Writing – review & editing, Methodology. **Mikko Voipio:** Writing – review & editing, Validation, Methodology, Formal analysis. **Senthil Kumar Rajendran:** Writing – review & editing, Methodology, Conceptualization. **John E. Eriksson:** Supervision, Methodology, Funding acquisition, Conceptualization.

Declaration of competing interest

Navid Delshad, Michael Santos Silva, Emrah Yatkin, and Mikko Voipio declare no conflict of interest. Preethy Paul, Senthil Kumar Rajendran, and John E Eriksson are co-founders of Anison Therapeutics Oy, which holds patents for pharmaceutical compositions of AA and OVT and the use thereof. All experimental procedures, data analysis, and interpretations in this manuscript were conducted with scientific rigor and objectivity, and the results are presented without bias.

Acknowledgments

This research was supported by the financial funds provided by JANE JA AATOS ERKO Foundation, and Tor, Joe and Pentti Borg's Memorial Fund.

We appreciate the personnel of the Central Animal Laboratory at the University of Turku and Admescope OY for their expertise in conducting *in vivo* studies and animal care. We would also like to acknowledge Anison Therapeutics for providing Anisomelic Acid and Ovatodiolide for research purposes. The graphical abstract and Fig. 6 (Proposed metabolic pathways of Anisomelic Acid and Ovatodiolide *in vivo*) were created in Biorender (Biorender.com).

Supplementary materials

Supplementary material associated with this article can be found, in the online version, at doi:10.1016/j.ejps.2025.107235.

Data availability

The dataset associated with this study is publicly available on Mendeley Data and can be accessed via the following link:https://%20https//doi.org/10.17632/my84g8d55b.1.

References

Al-Thubiani, W.S., 2023. The role of P-glycoprotein (P-gp) in cancer multidrug resistance (MDR): challenges for inhibiting P-gp in the context of overcoming MDR. J. Pharm. Res. Int. 35, 44–58. https://doi.org/10.9734/jpri/2023/v35i237422.

Bhuvaneshwari, R., Anandhan, R., 2024. A brief review on phytochemical constituent and pharmacological activities of Anisomeles malabarica (L.). Environ. Ecol. 42, 547–552. https://doi.org/10.60151/envec/RNSW4006.

Chang, H.L., Chen, H.A., Bamodu, O.A., Lee, K.F., Tzeng, Y.M., Lee, W.H., Tsai, J.T., 2018. Ovatodiolide suppresses yes-associated protein 1-modulated cancer stem cell phenotypes in highly malignant hepatocellular carcinoma and sensitizes cancer cells to chemotherapy *in vitro*. Toxicol. *In Vitro* 51, 74–82. https://doi.org/10.1016/j.tiv.2018.04.010.

Chen, J.C., Dai, Y.Z., Tzeng, Y.M., Liao, J.W., 2021. Genotoxicity and 28-day repeated dose oral toxicity study of ovatodiolide in rats. Toxicol. Rep. 8, 1783–1791. https://doi.org/10.1016/j.toxrep.2021.10.010.

de Souza, T.A., Pereira, L.H.A., Alves, A.F., Dourado, D., Lins, J.D.S., Scotti, M.T., Scotti, L., Abreu, L.S., Tavares, J.F., Silva, M.S., 2024. *Jatropha* diterpenes: an updated review concerning their structural diversity, therapeutic performance, and future pharmaceutical applications. Pharmaceuticals 17, 1399. https://doi.org/10.3390/ph17101399.

Emran, T.B., Shahriar, A., Mahmud, A.R., Rahman, T., Abir, M.H., Siddiquee, M.F.R., Ahmed, H., Rahman, N., Nainu, F., Wahyudin, E., Mitra, S., Dhama, K., Habiballah, M.M., Haque, S., Islam, A., Hassan, M.M., 2022. Multidrug resistance in cancer: understanding molecular mechanisms, immunoprevention and therapeutic approaches. Front. Oncol. 12. https://doi.org/10.3389/fonc.2022.891652.

Eriksson, J., Paul, P., Peuhu, E., Akbarsha, M.A., 2018. Pharmaceutical compositions of anisomelic acid and the use thereof. Patent EP2895162B1.

Fersht, A.R., Kirby, A.J., 1967. The hydrolysis of aspirin. Intramolecular general base catalysis of ester hydrolysis. J. Am. Chem. Soc. 89, 4857–4863. https://doi.org/10.1021/ja00995a007.

Hou, Y.Y., Wu, M.L., Hwang, Y.C., Chang, F.R., Wu, Y.C., Wu, C.C., 2009. The natural diterpenoid ovatodiolide induces cell cycle arrest and apoptosis in human oral squamous cell carcinoma Ca9-22 cells. Life Sci. 85, 26–32. https://doi.org/10.1016/j.lfs.2009.04.013.

Huang, Y.J., Huang, T.H., Yadav, V.K., Sumitra, M.R., Tzeng, D.T., Wei, P.L., Shih, J.W., Wu, A.T., 2020. Preclinical investigation of ovatodiolide as a potential inhibitor of colon cancer stem cells via downregulating sphere-derived exosomal β-catenin/STAT3/miR-1246 cargoes. Am. J. Cancer Res. 10, 2337–2354.

Hui, Z., Wen, H., Zhu, J., Deng, H., Jiang, X., Ye, X.Y., Wang, L., Xie, T., Bai, R., 2024. Discovery of plant-derived anti-tumor natural products: potential leads for anti-tumor drug discovery. Bioorg. Chem. 142, 106957. https://doi.org/10.1016/j.bioorg.2023.106957.

Lau, N., Phan, K., Mohammed, Y., 2024. Role of skin enzymes in metabolism of topical drugs. Metab. Target Organ Damage 4. https://doi.org/10.20517/mtod.2024.17. N/A-N/A.

Liu, S.C., Huang, C.M., Bamodu, O.A., Lin, C.S., Liu, B.L., Tzeng, Y.M., Tsai, J.T., Lee, W. H., Chen, T.M., 2019. Ovatodiolide suppresses nasopharyngeal cancer by targeting stem cell-like population, inducing apoptosis, inhibiting EMT and dysregulating JAK/STAT signaling pathway. Phytomedicine 56, 269–278. https://doi.org/10.1016/j.phymed.2018.05.007.

Lu, K.T., Wang, B.Y., Chi, W.Y., Chang-Chien, J., Yang, J.J., Lee, H.T., Tzeng, Y.M., Chang, W.W., 2016. Ovatodiolide inhibits breast cancer stem/progenitor cells through SMURF2-mediated downregulation of Hsp27. Toxins 8. https://doi.org/10.3390/toxins8050127.

OECD, 2002. Test No. 420: Acute Oral Toxicity–Fixed Dose Procedure. OECD. https://doi.org/10.1787/9789264070943-en. URL(accessed 6.27.25).

Ou, J., Meng, F., Liu, J., Li, D., Cao, H., Sun, B., 2020. Ovatodiolide exerts anticancer effects on human cervical cancer cells via mitotic catastrophe, apoptosis and inhibition of NF-kB pathway. J. BUON 25, 87–92.

Paul, P., Rajendran, S.K., Peuhu, E., Alshatwi, A.A., Akbarsha, M.A., Hietanen, S., Eriksson, J.E., 2014. Novel action modality of the diterpenoid anisomelic acid causes depletion of E6 and E7 viral oncoproteins in HPV-transformed cervical carcinoma cells. Biochem. Pharmacol. 89, 171–184. https://doi.org/10.1016/j.bcp.2014.02.011.

Potęga, A., 2022. Glutathione-mediated conjugation of anticancer drugs: an overview of reaction mechanisms and biological significance for drug detoxification and bioactivation. Molecules 27, 5252. https://doi.org/10.3390/molecules27165252.

Preethy, C.P., Alshatwi, A.A., Gunasekaran, M., Akbarsha, M.A., 2013. Analysis of the cytotoxic potential of anisomelic acid isolated from Anisomeles malabarica. Sci. Pharm. 81, 559–566. https://doi.org/10.3797/scipharm.1210-15.

Quantin, P., Stricher, M., Catoire, S., Ficheux, H., Egles, C., 2022. Dermatokinetics: advances and experimental models, focus on skin metabolism. Curr. Drug Metab. 23, 340–354. https://doi.org/10.2174/1389200223666220517114004.

Rajendran, S.K., Paul, P., Brusentsev, Y., Eklund, P., Eriksson, J., Sippola-Thiele, M., 2020. Pharmaceutical compositions of ovatodiolide and the use thereof. Patent CA3143889A1.

Santhanalakshmi, B., Sivanandhan, G., Manojkumar, S., Anitha, S., Sharmistha, G., Selvaraj, N., Kapildev, G., 2024. Ethnopharmacological potential of Anisomeles malabarica: a systematic review on traditional uses and bioactive compounds. Plant Biosyst. Int. J. Deal. Asp. Plant Biol. 158, 925–941. https://doi.org/10.1080/11263504.2024.2379365.

Senthilkumar, R., Brusentsev, Y., Paul, P., Marimuthu, P., Cheng, F., Eklund, P.C., Eriksson, J.E., 2019. Synthesis and evaluation of anisomelic acid-like compounds for the treatment of HPV-mediated carcinomas. Sci. Rep. 9, 20295. https://doi.org/10.1038/s41598-019-56410-1.

Senthilkumar, R., Karaman, D.Ş., Paul, P., Björk, E.M., Odén, M., Eriksson, J.E., Rosenholm, J.M., 2015. Targeted delivery of a novel anticancer compound anisomelic acid using chitosan-coated porous silica nanorods for enhancing the apoptotic effect. Biomater. Sci. 3, 103–111. https://doi.org/10.1039/c4bm00278d.

Wu, A.T.H., Srivastava, P., Yadav, V.K., Tzeng, D.T.W., Iamsaard, S., Su, E.C.Y., Hsiao, M., Liu, M.C., 2020. Ovatodiolide, isolated from Anisomeles indica, suppresses bladder carcinogenesis through suppression of mTOR/β-catenin/CDK6 and exosomal miR-21 derived from M2 tumor-associated macrophages. Toxicol. Appl. Pharmacol. 401, 115109. https://doi.org/10.1016/j.taap.2020.115109.

Xiang, J., Zhang, X., Wang, D., Li, J., Li, Q., Wang, Q., Ding, Y., Chen, T., Sun, Y., Bao, S., Chen, J., Li, D., Wang, L., Chen, Y., 2020. Chemical modification of ovatodiolide revealed a promising amino-prodrug with improved pharmacokinetic profile. Chem. Commun. 56, 11018–11021. https://doi.org/10.1039/c9cc07573a.

Zhang, L., Li, D., Chen, X., Zhao, F., 2025. Marine-derived diterpenes from 2019 to 2024: structures, biological activities, synthesis and potential applications. Mar. Drugs 23, 72. https://doi.org/10.3390/md23020072.